Chemistry & Biology
Article

# Arginine Topology Controls Escape of Minimally Cationic Proteins from Early Endosomes to the Cytoplasm

Jacob S. Appelbaum,[1,4] Jonathan R. LaRochelle,[3,4] Betsy A. Smith,[2,5] Daniel M. Balkin,[1] Justin M. Holub,[2] and Alanna Schepartz[2,3,*]
[1]Department of Cell Biology, Yale University School of Medicine, PO Box 208002, New Haven, CT 06520-8002, USA
[2]Department of Chemistry, Yale University, PO Box 208107, New Haven, CT 06520-8107, USA
[3]Department of Molecular, Cellular, and Developmental Biology, Yale University, PO Box 208103, New Haven, CT 06520-8103, USA
[4]These authors contributed equally to this work
[5]Present address: Department of Chemistry, Princeton University, Princeton, NJ 08544, USA
*Correspondence: alanna.schepartz@yale.edu
http://dx.doi.org/10.1016/j.chembiol.2012.05.022

## SUMMARY

**Proteins represent an expanding class of therapeutics, but their actions are limited primarily to extracellular targets because most peptidic molecules fail to enter cells. Here we identified two small proteins, miniature protein 5.3 and zinc finger module ZF5.3, that enter cells to reach the cytosol through rapid internalization and escape from Rab5+ endosomes. The trafficking pathway mapped for these molecules differs from that of Tat and $Arg_8$, which require transport beyond Rab5+ endosomes to gain cytosolic access. Our results suggest that the ability of 5.3 and ZF5.3 to escape from early endosomes is a unique feature and imply the existence of distinct signals, encodable within short sequences, that favor early versus late endosomal release. Identifying these signals and understanding their mechanistic basis will illustrate how cells control the movement of endocytic cargo and may allow researchers to engineer molecules to follow a desired delivery pathway for rapid cytosolic access.**

## INTRODUCTION

Protein represent a rapidly expanding class of therapeutic molecules (Strohl and Knight, 2009), but their actions are limited primarily to extracellular targets (Fischer, 2007; Johnson et al., 2011) because the size and composition of most polypeptides and peptide mimetics preclude their uptake into mammalian cells (Luedtke et al., 2003). It has been known for over 40 years that addition of cationic charges to a peptide or protein can aid transport into cells (Ryser and Hancock, 1965), and many reports have documented the utility of appending basic sequences derived from the HIV transactivator of transcription (Tat) (Zhou et al., 2009), *D. melanogaster* Antennapedia (Théodore et al., 1995), or simply polyarginine (for example, $Arg_8$) (Futaki et al., 2001) to peptides or small molecules (Wender et al., 2008) to increase their cytoplasmic access. Certain highly positively charged proteins (Cronican et al., 2011) and toxins (Johannes and Popoff, 2008) and certain peptide mimetics (Verdine and Hilinski, 2012; White et al., 2011) also possess cell-penetrating properties, but it remains unknown how one can leverage these examples to control the precise entry pathway or enhance the uptake of designed peptides or mimetics.

Two contrasting mechanisms have been proposed for the cytosolic entry of cationic proteins and related molecules. The first (ion-pair-guided passive diffusion) posits that guanidinium side chains on the polypeptide form hydrogen bonds with cell-surface phospholipids creating neutral ion pairs that passively diffuse across the plasma membrane (Rothbard et al., 2005). The second model (endosomal release) asserts that endocytosis is a major portal through which cationic polypeptides and peptide mimetics enter the cell (Fischer, 2007). Previous investigations have attempted to distinguish between these two models by blocking endocytosis via thermal (Derossi et al., 1996), pharmacologic (Wadia et al., 2004; Fischer et al., 2004), or genetic means (Ter-Avetisyan et al., 2009). The interpretation of these experiments is complicated, however, by differences in protein/polypeptide concentration and analytical method. For example, incubation of living cells with cationic proteins/polypeptides at concentrations $\geq$10 μM leads to the formation of nucleation zones (Duchardt et al., 2007) that transiently disrupt membranes (Palm-Apergi et al., 2009), causing the spontaneous release of peptide into the cytosol. Incubation of cells at lower concentrations ($\leq$5 μM) of peptide, in the presence of drugs that inhibit endocytosis, prevents cytoplasmic access (Wadia et al., 2004), implying that at low concentrations, the molecules studied cannot diffuse through the plasma membrane. Moreover, the many studies using microscopy to examine cells fixed by treatment with formaldehyde or methanol must be reevaluated in light of evidence that the fixation process can release fluorescently labeled peptides from endosomes (Belitsky et al., 2002 and Richard et al., 2003), an artifact not observed during microscopic examination of living cells. Finally, the high-intensity light used during microscopy can itself facilitate the redistribution of fluorescently labeled peptides from endosomes to cytoplasm (Maiolo et al., 2004). Thus, whether, when, and how these cationic molecules escape endocytic vesicles to access the cytosol remain unanswered questions.

Attempts to identify the structural determinants of cell permeability are complicated by the above experimental details, as well as by the fact that neither Tat nor $Arg_8$ possesses a defined fold. Miniature proteins are a family of small (36 aa), well-folded polypeptides that adopt a characteristic hairpin fold consisting of axially packed α- and PPII helices (Blundell et al., 1981; Hodges and Schepartz, 2007). Miniature proteins identified through both rational design (Zondlo and Schepartz, 1999; Zellefrow et al., 2006) and molecular evolution (Chin and Schepartz, 2001; Rutledge et al., 2003; Golemi-Kotra et al., 2004; Gemperli et al., 2005) can modulate protein function by inhibiting protein interactions (Rutledge et al., 2003; Gemperli et al., 2005); both loss-of-function and gain-of-function activities have been observed (Golemi-Kotra et al., 2004; Gemperli et al., 2005; Zellefrow et al., 2006). We reported previously that minimally cationic miniature proteins containing between 2 and 6 arginine residues embedded within the α- or PPII helix were taken up by mammalian cells in culture more efficiently than Tat or $Arg_8$ (Daniels and Schepartz, 2007; Smith et al., 2008). In this report we investigate whether, when, and how miniature proteins containing arginine access the cytoplasm.

To learn more about the structural determinants of cytoplasmic access, we designed a set of miniature proteins that differed in the number and density of α-helical arginine side chains and tracked their passage into the cell. Using low concentrations (1 μM) of fluorophore-conjugated variants, we found that a minimum of four α-helical arginines was required for cell uptake, and that uptake was enhanced when the arginines were clustered on the same α-helix face. Next, a novel and rapid assay for evaluating cytoplasmic access revealed that of four cationic miniature proteins taken up by cells, only one reaches the cytosol. This miniature protein, which we named 5.3, possesses a distinct array of five dispersed α-helical arginines. Live-cell confocal microscopy revealed that rhodamine-labeled 5.3 ($5.3^R$) is taken up by an endocytic pathway that includes Rab5+ and Rab7+ endosomes. This pathway is shared by Tat, $Arg_8$, and cationic miniature proteins that do not reach the cytosol. However, for 5.3, Tat, or $Arg_8$ to gain cytosolic access, active endocytosis and endosomal acidification were required. We find further that unlike Tat or $Arg_8$, which require vesicle maturation beyond the Rab5+ stage, miniature protein 5.3 accesses the cytosol by crossing specific membrane regions present in early Rab5+ endosomes. Finally, grafting the arginine array present in 5.3 into a well-folded zinc finger domain (Krizek et al., 1991) successfully endowed this domain with the trafficking properties of 5.3. These experiments demonstrate that discrete arginine arrangements embedded within a well-folded protein can direct cytosolic access by facilitating both efficient uptake and early endosomal escape.

## RESULTS

### Miniature Protein Design

To examine the effect of charge density and orientation on cell uptake, we prepared eight miniature proteins containing between one and six arginine residues at various positions on the solvent-exposed α-helical surface of the hairpin fold. These molecules also contained two arginines near the C terminus (Figure 1A). Seven of these cationic miniature proteins were characterized by circular dichroism (CD) spectra at 37°C that were virtually indistinguishable from that of the parent molecule lacking additional arginines, aPP (Figure S1A available online). The CD spectra of six were temperature-dependent with cooperative transitions between 49°C and 67°C (Figures S1B and S1C), suggesting that they each retained a stable and characteristic hairpin fold (Hodges and Schepartz, 2007). Miniature protein 6.3, containing the greatest number of arginine substitutions (six), showed reduced ellipticity at 222 nm and 208 nm (Figure S1A), along with a reduced $T_m$ of 33°C (Figures S1B and S1C); 6.3 was not studied further. For the remaining molecules, these CD data suggest that arginine substitution does not significantly alter miniature protein secondary structure, and that Figure 1B is a reasonable representation of the arginine side-chain arrangement in miniature proteins 2.1, 2.2, 3.2, 4.2, 4.3, 5.2, and 5.3.

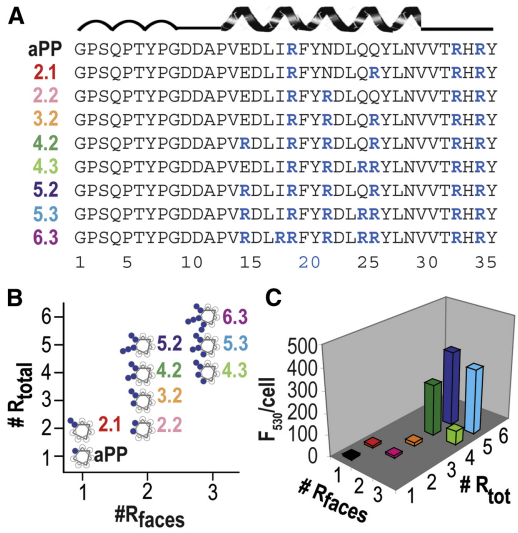


**Figure 1. Miniature Protein Design**

(A) Sequences of minimally cationic miniature proteins evaluated in this work.

(B) A plot of the relationship between the total number of α-helical arginine residues (# $R_{total}$) and the number of α-helical faces on which these arginines are displayed (# $R_{faces}$) for each aPP variant. The location of each α-helical arginine residue is represented by a blue circle on the helical wheel.

(C) A plot of mean cellular fluorescence at 530 nm of HeLa cells treated with fluorescently tagged miniature protein variants (5 μM, 30 min).

See also Figure S1.

### Cell Uptake

Initially we used flow cytometry to assess the influence of arginine number and orientation on miniature protein uptake. In preliminary studies, we evaluated molecules labeled with fluorescein on their C-termini (as denoted with superscript F). To ensure that our experiment measured miniature proteins that had entered cells, we included a trypsin wash just before analysis via flow cytometry. Treatment of HeLa cells with 5 μM $aPP^F$, $2.1^F$, $2.2^F$, or $3.2^F$ resulted in only small increases (<3-fold) in cell fluorescence, while treatment with $4.2^F$, $4.3^F$, $5.2^F$, or $5.3^F$ resulted in increases in cell fluorescence between 7- and 40-fold (Figure 1C). We therefore chose to focus on miniature proteins showing significant uptake and confirmed

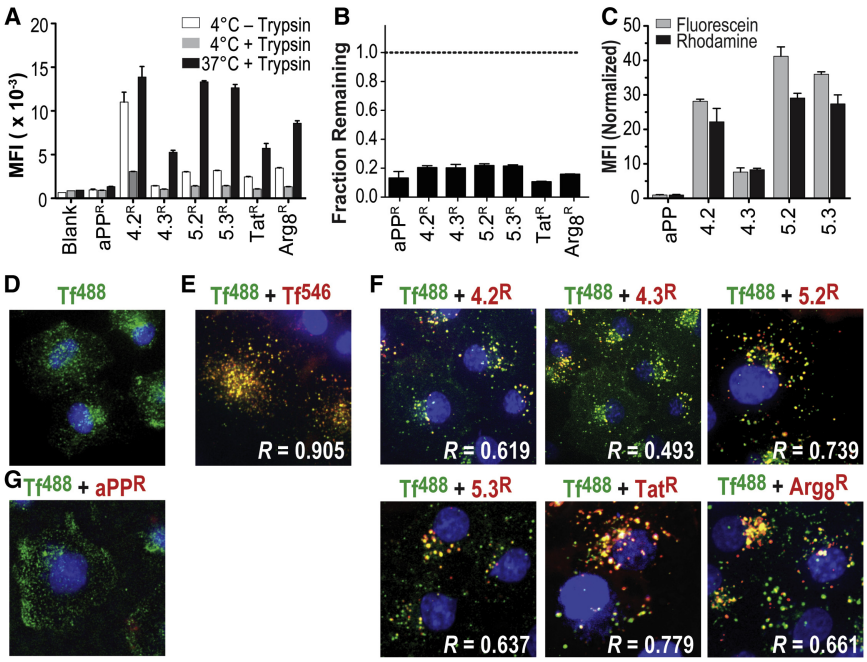


**Figure 2. Arginine Topology Controls Cell Binding and Uptake**

(A) Evaluation of cell surface binding of rhodamine-labeled cationic miniature proteins and peptides in the absence of endocytosis and removal by trypsin treatment. HeLa cells were treated with 1 μM of the indicated rhodamine-labeled molecule for 30 min. Cell were then treated with trypsin (0.05%, 10 min, 37°C) or PBS before washing and analysis by flow cytometry. MFI, mean fluorescent intensity.

(B) Fraction of cell-associated fluorescence remaining after trypsin treatment. These data represent the ratio of black to grey bars shown in (A).

(C) Comparison of the relative uptake by HeLa cells of the indicated rhodamine- and fluorescein-labeled miniature proteins (black and gray bars, respectively) after 30 min. The MFI for each sample is shown normalized to a control sample treated with aPP labeled with the same fluorophore. The mean ± SE is shown.

(D–F) When added to HeLa cells, AlexaFluor-488-transferrin ($Tf^{488}$) (D) colocalizes with AlexaFluor-546-labeled transferrin ($Tf^{546}$) (E) and rhodamine-labeled miniature proteins and peptides (F). Perfect colocalization is characterized by a Pearson's R value (R) equal to 1, while R values near 0 represent little or no colocalization. The correlation value observed when cells were treated with both $Tf^{488}$ and $Tf^{546}$ is 0.905.

(G) When added with $Tf^{488}$, $aPP^R$ shows little intracellular signal. Rhodamine-labeled cationic miniature proteins and $Tf^{546}$ are shown in red, $Tf^{488}$ is shown in green, and Hoescht (nucleus) is shown in blue.

Error bars shown represent mean ± SE. See also Figure S2.

these results by synthesizing analogs labeled instead with tetraethyl rhodamine sulfate (denoted with superscript R), a dye with several desirable properties, including resistance to photobleaching and an emission spectrum unaffected by pH changes and far from the autofluorescence spectrum of cells (Fernández-Suárez and Ting, 2008). As found for miniature proteins labeled with fluorescein, rhodamine-labeled miniature proteins containing four or five α-helical arginines were taken up efficiently, in some cases ($5.2^R$ and $5.3^R$) more efficiently than $Tat^R$ or $Arg_8^R$ (Figure 2A).

Because previous studies have shown that cell-penetrating peptides, including Tat and $Arg_8$, bind to cell-surface proteoglycans (Payne et al., 2007), we verified that trypsin treatment removed miniature proteins that were bound to the cell surface. Peptides and proteins that enter the cell are inaccessible to trypsin added to the culture media (Frankel and Pabo, 1988). Therefore, we arrested membrane traffic by incubating cells at 4°C (Hanover et al., 1984; Vonderheit and Helenius, 2005) for 15 min prior to and during a 30 min treatment with 1 μM $4.2^R$, $4.3^R$, $5.2^R$, $5.3^R$, $Tat^R$, $Arg_8^R$, or $aPP^R$. After incubation, cells were washed with PBS and incubated with 0.05% trypsin or PBS (as a control) before analysis by flow cytometry. These results were compared to those obtained when cells were incubated at 37°C and treated with trypsin (Figure 2A). Cationic miniature proteins $4.2^R$, $4.3^R$, $5.2^R$, and $5.3^R$ bound to cells between 2.7-fold and 35-fold more than $aPP^R$ and in some cases ($5.2^R$ and $5.3^R$) to an extent comparable to that of $Tat^R$ and $Arg_8^R$. For cells incubated at 4°C, trypsin treatment decreased the fluorescent signal between 77% and 89% (Figure 2B). These data confirm that at 4°C, incubation of cells with 1 μM cationic miniature protein leads to little if any cell uptake, and confirms that the vast majority of material bound to the cell surface is degraded and/or effectively removed by trypsin treatment. Comparison of the uptake of rhodamine- and fluorescein-labeled miniature proteins (Figure 2C) shows that cell uptake depends on arginine density: miniature proteins containing four arginine residues clustered on two helical faces were taken up more efficiently than those containing four arginines on three helical faces (Figures 1C, 2A, and 2C). Molecules containing five α-helical arginines were taken up to a similar extent, irrespective of density, revealing that among these molecules the impact of arginine arrangement was smaller. Consistent with our previous work (Smith et al., 2008), the cationic miniature proteins $5.2^R$ and $5.3^R$ are taken up with an efficiency ≥2-fold better than that of Tat or $Arg_8$, despite the fact that they possess twice the mass and fewer (7 rather than 8) positive charges.

## Cationic Miniature Proteins Traffic First into Endocytic Vesicles

To better understand the uptake pathway, we treated HeLa cells with rhodamine-labeled miniature proteins in the presence of transferrin labeled with AlexaFluor-488 ($Tf^{488}$) and quantified fluorescence overlap using confocal microscopy. Transferrin is rapidly internalized from the plasma membrane into endocytic vesicles (Hanover et al., 1984; Lakadamyali et al., 2006), and observing transferrin within rhodamine+ vesicles would suggest that the vesicles were endocytic in nature, originating from the plasma membrane. We incubated HeLa cells for 30 min with $Tf^{488}$ (25 nM) and 1 μM $4.2^R$, $4.3^R$, $5.2^R$, $5.3^R$, $Tat^R$, or $Arg_8^R$ before washing with media, staining with Hoescht (to visualize

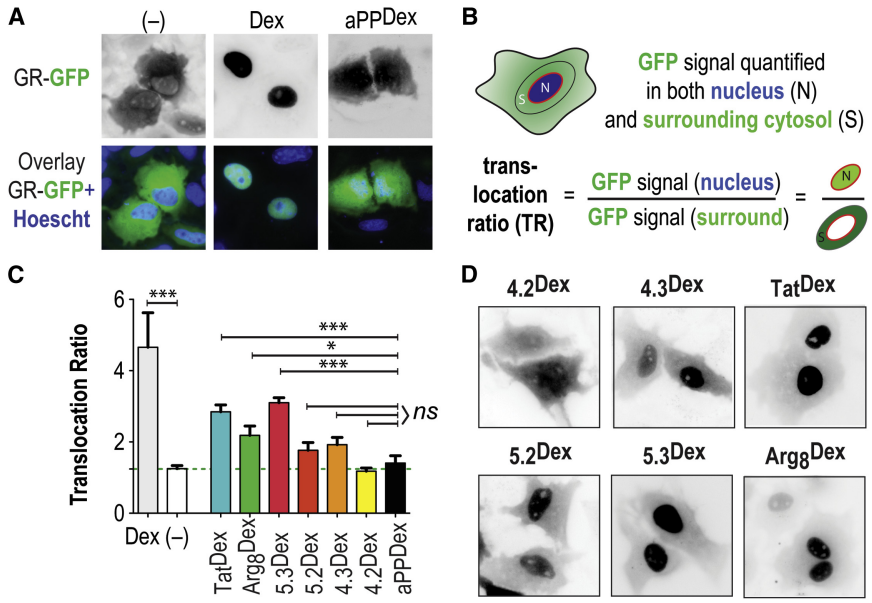


**Figure 3. Translocation of GR-GFP after Treatment with Dexamethasone and Certain Dexamethasone-Labeled Miniature Proteins and Peptides**

(A) HeLa cells transfected with GR-GFP (which appears black in the top row) after no treatment (–) or treatment with 1 μM dexamethasone (Dex) or 1 μM aPP$^{Dex}$ for 30 min at 37°C. The lower panel is an overlay of the GFP signal, shown in green, and the nuclear Hoescht signal, shown in blue.

(B) Quantification scheme.

(C) Quantification of the changes visible in (D). *ns*, not significant; *p ≤ 0.05, ***p ≤ 0.001, ANOVA. See also Figure S3.

(D) Visualization of the change in GR-GFP localization after treatment with 1 mM Dex-labeled miniature protein or peptide for 30 min.

DNA), and imaging without fixation by confocal microscopy (Figures 2D–2F). Cells treated with Tf$^{488}$ showed small, discrete areas of intense green fluorescent signal. Treatment with aPP$^{R}$ led to little or no red fluorescent signal (Figure 2G), confirming earlier results showing that aPP$^{R}$ is not taken up efficiently. By contrast, HeLa cells treated with 1 μM 4.2$^{R}$, 4.3$^{R}$, 5.2$^{R}$, 5.3$^{R}$, Tat$^{R}$, or Arg$_8$$^{R}$ showed red fluorescent puncta throughout the cytosol in a distribution similar to that seen with Tf$^{488}$ and at levels that qualitatively reproduce the trends detected by flow cytometry (Figure 2F). The fluorescent signals from Tf$^{488}$ and Tf$^{546}$ were highly correlated (Figure 2E), as were, with one exception, the fluorescent signals from Tf$^{488}$ and rhodamine-labeled miniature proteins/peptides ($R_{488,rhodamine}$ = 0.619–0.779). Taken together, these data suggest that transferrin and cationic miniature proteins/peptides 4.2$^{R}$, 5.2$^{R}$, 5.3$^{R}$, Tat$^{R}$, and Arg$_8$$^{R}$ are taken up into the same endocytic compartments. Miniature protein 4.3$^{R}$ is also taken up into a transferrin+ compartment, but the correlation ($R_{488,rhodamine}$ = 0.493) is lower, possibly because the uptake is low (Figure 2F). Additional experiments to assess whether peptide trafficking was affected by fluorophore identity confirmed that rhodamine- and fluorescein-labeled variants of cationic miniature proteins, as well as Tat and Arg$_8$, traffic together within cells, as indicated by highly correlated rhodamine and fluorescein intensities ($R$ > 0.6, p < 1 × 10$^{-10}$; Figure S2).

## Certain Cationic Miniature Proteins Reach the Cytoplasm

Polypeptides and peptide mimetics showing cellular uptake by flow cytometry may remain trapped in endosomes and fail to reach the cytosol (Yu et al., 2011 and Maiolo et al., 2004). Previous assays for the cytosolic localization of peptide- or peptoid-dexamethasone (Dex) conjugates exploited the interaction of the Dex-labeled molecule with the ligand-binding domain of the cytosolic glucocorticoid receptor (GR), which led eventually to the transcription of luciferase and its detection in cell lysates 40–48 hr later (Yu et al., 2005). Recognizing that treatment of cells with Dex leads to rapid (15 min) nuclear accumulation of a GR-green fluorescent protein fusion (GR-GFP) (Carey et al., 1996), we asked whether microscopy could provide a rapid assay for cytosolic localization by revealing the nuclear accumulation of GR-GFP in the presence of peptide-Dex conjugates.

To test this hypothesis, HeLa cells transiently transfected with GR-GFP were incubated for 30 min with between 0 and 10 μM Dex (Figure 3A and Figure S3A). When Dex was absent from the incubation media, these cells exhibited GFP signal throughout the cytoplasm and the nucleus (Figure 3A). Addition of between 3 nM and 10 μM Dex led to a dose-dependent decrease in the cytosolic GFP signal and a concomitant increase in the nuclear GFP signal (Figure S3A). We quantified these changes using the automated image processing package CellProfiler (Carpenter et al., 2006) to measure the ratio of the median GFP signal in the nucleus to the median signal within a 2 μm region surrounding the region of cytosol (the "translocation ratio" [TR]; Figure 3B). TR values near 1 indicate equivalent intensity between the nucleus and the surrounding region. Treatment of HeLa cells with 1 μM Dex for 30 min resulted in an increase in the TR from 1.07 ± 0.02 to 3.93 ± 0.14 (p = 1.92 × 10$^{-22}$, versus untreated cells, two-tailed t test), roughly 90.5% of the value achieved with a 10-fold higher concentration (Figure 3C). We therefore chose the lower concentration for subsequent studies. When cells transfected with GR-GFP were treated for 30 min with 1 μM aPP$^{Dex}$, virtually no change in GR-GFP localization or the TR was observed (1.41 ± 0.09 versus 1.25 ± 0.04, p = 0.1473; two-tailed t test; Figures 3A and 3C). These data are consistent with the observation that aPP$^{R}$ fails to enter cells and with previous results (Yu et al., 2005) showing that simply adding the Dex label does not confer upon an otherwise cell-impermeable peptide the ability to reach the cytoplasm.

We next evaluated the extent to which Dex-labeled miniature proteins, as well as Tat and Arg$_8$, induce the nuclear translocation of GR-GFP (Figures 3C and 3D). Treatment of HeLa cells expressing GR-GFP with 1 μM 5.3$^{Dex}$ for 30 min led to a large increase in TR (3.1 ± 0.1) compared to both an untreated sample (–) (p = 2.68 × 10$^{-48}$, ANOVA with Bonferroni post-test) and one

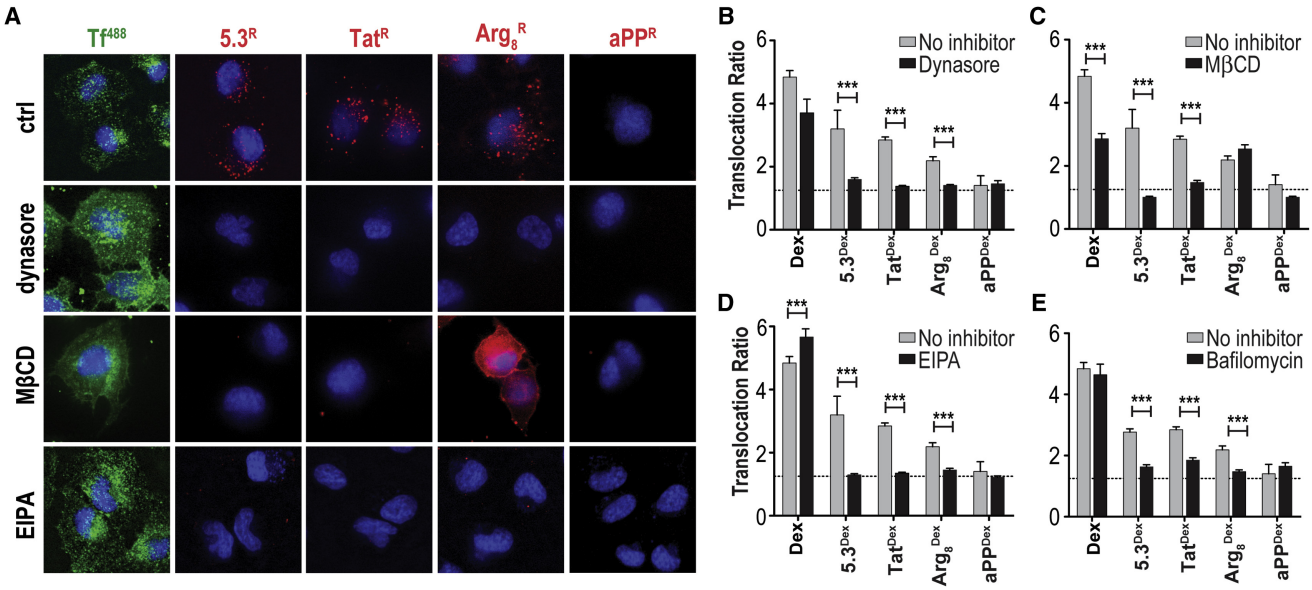


**Figure 4. Endocytosis Is Required for Cytosolic Access**

(A) Confocal microscopy images of HeLa cells treated with the indicated rhodamine- or AlexaFluor488-labeled peptide or miniature protein and various endocytosis inhibitors.

(B–E) Translocation ratio after treatment of HeLa cells with 1 μM Dex, 5.3Dex, TatDex, Arg8Dex, or aPPDex in the presence (black bars) or absence (gray bars) of various inhibitors of endocytosis, including 80 μM dynasore (B), 5 mM methyl-β-cyclodextrin (MβCD) (C), 50 μM EIPA (D), and 200 nM bafilomycin (E). *$p \leq 0.05$; ***$p \leq 0.001$, ANOVA with Bonferroni post-test. Error bars shown represent mean ± SE.

See also Figure S4.

treated with $aPP^{Dex}$ ($p = 1.96 \times 10^{-16}$). Treatment of cells with 1 μM $4.2^{Dex}$, $4.3^{Dex}$, or $5.2^{Dex}$ for 30 min led to a small or absent increase in nuclear GFP signal, and to TRs (1.18 ± 0.04, 1.92 ± 0.10, and 1.77 ± 0.11, respectively) that were not significantly different from those of cells treated with $aPP^{Dex}$. The TRs measured after treatment of cells with $Arg_8^{Dex}$ (2.19 ± 0.13) or $Tat^{Dex}$ (2.85 ± 0.10) showed an increase over those of control samples treated with $aPP^{Dex}$ ($Arg_8^{Dex}$, $p = 0.0053$; $Tat^{Dex}$, $p = 2.54 \times 10^{-9}$), and they were comparable to those of cells treated with $5.3^{Dex}$. Control experiments verified that the affinities of Dex-labeled cationic miniature proteins and peptides for the human glucocorticoid receptor in vitro were similar (between 1 and 36 nM), though they were all slightly poorer than Dex itself (0.1 nM, see Figures S3B–S3G).

We considered that degradation of miniature proteins could lead to GR-GFP activation through release of the Dex moiety. While $aPP^R$, $5.2^R$, and $5.3^R$ are cleaved by cathepsin D (and to a smaller extent cathepsin L) in vitro (Figures S6D–S6F), high-performance liquid chromatography analysis of whole-cell lysates revealed minimal to no cleavage of the $aPP^R$ and $5.3^R$ backbones in cells under the conditions of the translocation assay (Figures S3H and S3I). The stability of $aPP^R$ and $5.3^R$ under these conditions minimizes the possibility that the increased TR observed in the presence of $5.3^{Dex}$ results from increased degradation or protease susceptibility of this protein compared to $aPP^{Dex}$ or $5.2^{Dex}$. To further validate the results of the translocation assay, we generated cytoplasmic extracts from HeLa cells treated with rhodamine-labeled miniature proteins using streptolysin O (SLO) (Androlewicz et al., 1993). High-performance liquid chromatography analysis of the SLO extracts from HeLa cells treated with $aPP^R$ showed little to no fluorescent material, while analysis of cytoplasmic extracts from HeLa cells treated with $5.3^R$ confirmed the presence of intact $5.3^R$ (Figures S6D–S6E). Analysis of cytoplasmic extracts from HeLa cells treated with $Tat^R$ or $Arg_8^R$ also showed fluorescent material, but with retention times distinct from that of the starting material (Figures S6G and S6H), consistent with previous observations (Palm et al., 2007) that unstructured cell-penetrating peptides can be rapidly degraded. Cytoplasmic SLO extracts contained 4.4% of the 5.3R present within whole cell extracts (comparing data in Figure S3I with Figure S6E), while SLO extracts of HeLa cells treated with aPPR showed no detectable material (lower limit of detection = 0.5%; Figure S6D).

## Cytoplasmic Access Requires Active Endocytosis

Two limiting models have been invoked to explain the trafficking of cationic peptides and proteins across the plasma membrane and into the cytoplasm. One model invokes ion-pair-guided passive membrane diffusion (Rothbard et al., 2005); the other invokes endocytosis followed by endosomal release. We sought to distinguish between these models in two ways. First, we asked whether inhibitors of endocytosis block the uptake of cationic miniature proteins, their cytosolic localization, or both (Figure 4). Second, we confirmed that cell-membrane integrity is not disrupted by the presence of 1 μM cationic miniature protein (Figure S4).

To determine whether active endocytosis is required for $5.3^{Dex}$ to reach the cytoplasm, we treated HeLa cells expressing GR-GFP with inhibitors of endocytosis before and during exposure to 1 μM $5.3^{Dex}$. Clathrin-mediated endocytosis (CME),

pinocytosis, and caveolin-mediated endocytosis are dependent on dynamin (Doherty and McMahon, 2009), whose activity is inhibited by the small molecule dynasore (Macia et al., 2006). Depleting cellular cholesterol by treatment with methyl-β-cyclodextrin (MβCD) also inhibits these three processes (Rodal et al., 1999). Actin remodeling, a process inhibited by addition of N-ethyl-isopropyl amiloride (EIPA) (Koivusalo et al., 2010) facilitates clathrin-coated pit formation (Doherty and McMahon, 2009) and is required for some dynamin- and cholesterol-independent endocytic pathways. Notably, addition of EIPA does not block the uptake of some CME ligands such as transferrin (Koivusalo et al., 2010).

To test the involvement of these pathways in the uptake of cationic miniature proteins and peptides, we pretreated HeLa cells for 30 min with 80 μM dynasore, 5 mM MβCD, or 50 μM EIPA before adding 1 μM $aPP^{R}$, $5.3^{R}$, $Tat^{R}$, or $Arg_8^{R}$ for 30 min at 37°C in the presence of inhibitor. The cells were subsequently washed and visualized by confocal microscopy (Figure 4A). The presence of dynasore completely blocked the uptake of $5.3^{R}$, as well as $Tat^{R}$ and $Arg_8^{R}$, suggesting that all three molecules are taken up in a dynamin-dependent fashion. The presence of EIPA also dramatically reduced the uptake of all three molecules, suggesting a role for actin metabolism in the internalization process. MβCD completely blocked the uptake of $5.3^{R}$ and $Tat^{R}$, but not $Arg_8^{R}$. Surprisingly, cellular uptake of $Arg_8^{R}$ was increased in the presence of MβCD, leading to diffuse fluorescence throughout the cytosol, a pattern not observed in the absence of the inhibitor.

We next measured the effect of blocking endocytosis on the ability of $5.3^{Dex}$, $Tat^{Dex}$, and $Arg_8^{Dex}$ to reach the cytoplasm. We were mindful that exchanging the rhodamine label for Dex could alter the physical properties of the molecule, as well as the manner in which it trafficked in cells. HeLa cells transfected with GR-GFP were pretreated for 30 min with the same inhibitors prior to the addition of 1 μM of either Dex (positive control), $aPP^{Dex}$ (negative control), $5.3^{Dex}$, $Tat^{Dex}$, or $Arg_8^{Dex}$ for 30 min at 37°C (Figures 4B–4D). The cells were then washed and imaged to measure the TR. None of the endocytosis inhibitors altered the TR calculated for cells treated with $aPP^{Dex}$. However, all three inhibitors reduced to background levels the TR calculated after treatment with $5.3^{Dex}$ or $Tat^{Dex}$, and both dynasore and EIPA reduced the TR observed after treatment with $Arg_8^{Dex}$. As anticipated from the microscopy results discussed above, the cytoplasmic access of $Arg_8^{Dex}$ was not decreased in the presence of MβCD. Neither EIPA nor dynasore blocked the increase in the TR calculated after treatment with Dex, but MβCD reduced this increase by 53%, presumably the result of direct complexation of free Dex by MβCD (Moya-Ortega et al., 2010). The results with $Arg_8^{R}$ notwithstanding, these data support the contribution of endocytic pathways to the uptake of cationic miniature proteins and peptides, and not a model based on passive diffusion.

An endosome's acidification begins almost immediately upon its scission from the plasma membrane, as its lumen no longer communicates with the surrounding media. Bafilomycin is a potent inhibitor of the vesicular ATPase (Yoshimori et al., 1991), and its addition to culture media prevents endosomal acidification (Yoshimori et al., 1991; Fischer et al., 2004). To determine whether low vesicular pH was required for endosomal escape, we pretreated HeLa cells expressing GR-GFP with 200 nM bafilomycin for 1 hr before exposing them to 1 μM Dex, $5.3^{Dex}$, $Tat^{Dex}$, $Arg_8^{Dex}$, or $aPP^{Dex}$ (Figure 4E). Treatment with bafilomycin did not alter the effect of Dex or $aPP^{Dex}$ on the TR, but it completely blocked the increase in TR seen after cells were exposed to $5.3^{Dex}$ ($p = 1.4 \times 10^{-11}$), $Tat^{Dex}$ ($p = 5.3 \times 10^{-11}$), or $Arg_8^{Dex}$ ($p = 8.2 \times 10^{-6}$). Thus, while $5.3^{Dex}$, $Tat^{Dex}$, and $Arg_8^{Dex}$ reach the cytoplasm, they fail to do so in the absence of endosome acidification. This finding further supports the model that these molecules do not penetrate the plasma membrane directly, but rather escape to the cytoplasm from acidified endocytic vesicles.

## Escape to the Cytoplasm from Early Endosomes

Phospholipids present in newly formed clathrin-coated vesicles and macropinosomes undergo rapid modification resulting in the recruitment of Rab5 (Lakadamyali et al., 2006; Zoncu et al., 2009). Rab5 is a master regulator of endosome biogenesis (Zeigerer et al., 2012) and recruits additional cellular factors required for vesicle maintenance, fusion, and maturation, including the phosphatidyl inositol (PI) 3-OH kinase (PI3K) Vps34 (Christoforidis et al., 1999b). The resulting early endocytic compartment mixes via homotypic fusion with other Rab5+ vesicles (Stenmark et al., 1994) and delivers cargo to other cellular locales through the budding off of transport vesicles (Puthenveedu et al., 2010) or Rab conversion (Rink et al., 2005). While some cargo (such as transferrin) is recycled to the cell surface, other cargo, such as low-density lipoprotein, epidermal growth factor (Cantalupo et al., 2001), and several types of virus (Vonderheit and Helenius, 2005) are delivered to late endosomes, marked by Rab7, for degradation in lysosomes (Huotari and Helenius, 2011). To characterize the intracellular route taken by $5.3^{R}$, $Tat^{R}$, and $Arg_8^{R}$, we looked for overlap of these molecules with markers of endocytic uptake and GFP-tagged Rab proteins. We also used small molecule inhibitors and dominant-negative Rab variants to test the cellular activities required for $5.3^{Dex}$, $Tat^{Dex}$, and $Arg_8^{Dex}$ to enter the cytoplasm.

Guided by the observation that $5.3^{R}$ colocalizes with transferrin (Figure 3), a substrate known to internalize into Rab5+ vesicles (Lakadamyali et al., 2006), we asked whether $5.3^{R}$ was also present in Rab5+ vesicles. HeLa cells were transfected with GFP-Rab5 and treated for 30 min with 1 μM $5.3^{R}$. When these cells were examined by confocal microscopy, 66% of the rhodamine signal overlapped with the signal from GFP-Rab5, confirming that $5.3^{R}$ is present in Rab5+ vesicles (Figure 5A). Because Rab5 vesicles rapidly deliver their cargo to downstream vesicles (Rink et al., 2005), we also evaluated colocalization of $5.3^{R}$ with Rab7-GFP (Figure 5C). HeLa cells transfected with Rab7-GFP and treated with $5.3^{R}$ as above showed a large fraction (87%) of the rhodamine signal located in the Rab7-GFP compartment, confirming that $5.3^{R}$ enters both early (Rab5+) and late (Rab7+) endosomes. We found no overlap between $5.3^{R}$, $Tat^{R}$, or $Arg_8^{R}$ and galT-GFP (Cole et al., 1996), a marker of the golgi (Figure S5). To test whether trafficking of $5.3^{R}$ could be arrested at the Rab5 stage, we overexpressed a GTPase-inactive Rab5 mutant, $Rab5^{Q79L}$ (Stenmark et al., 1994), that blocks delivery of cargo to late endosomes and arrests vesicle maturation (Rink et al., 2005). Observation of HeLa cells transfected with $Rab5^{Q79L}$-GFP and

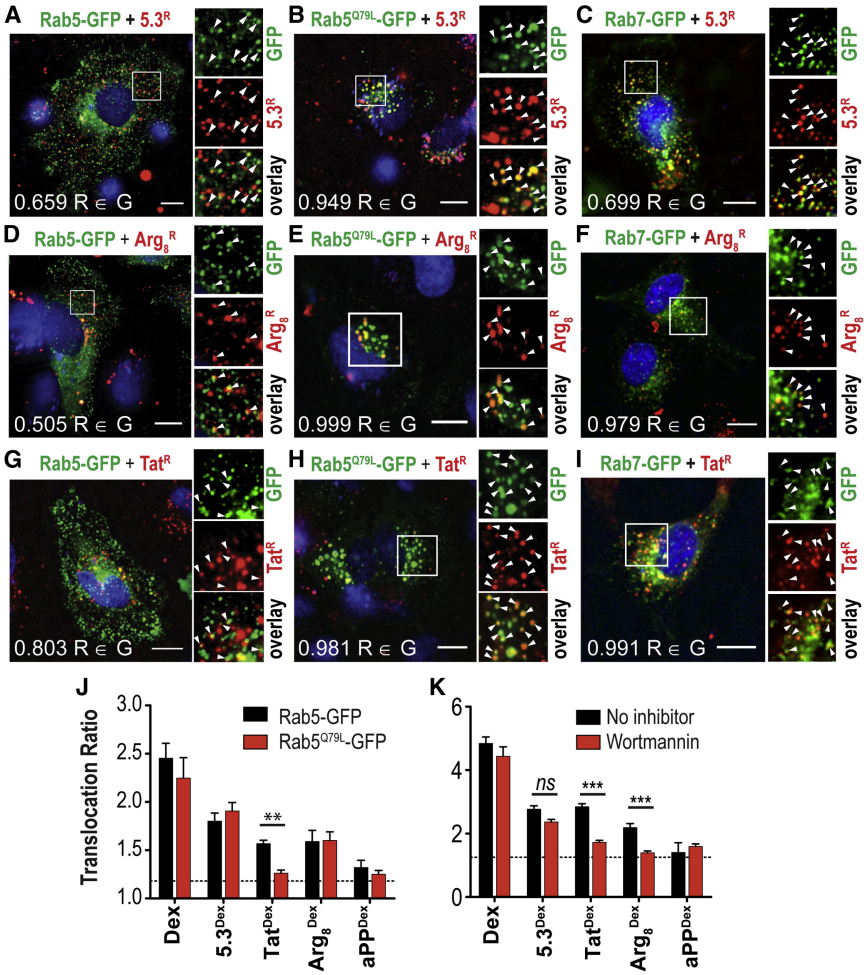


**Figure 5. Differential Trafficking and Release of Miniature Protein 5.3, Tat, and Arg8**

(A–I) HeLa cells transfected with the indicated GFP fusion protein were treated with 1 μM $5.3^R$ (A–C), $Arg8^R$ (D–F), or $Tat^R$ (G–I) before being washed and imaged by confocal microscopy. Colocalization of $5.3^R$, $Tat^R$, and $Arg_8^R$ with Rab5-GFP is moderate ([A], [D], and [G]) but can be increased by arresting Rab5 maturation via overexpression of $Rab5^{Q79L}$-GFP ([B], [E], and [H]. $5.3^R$, $Tat^R$, and $Arg_8^R$ are delivered to Rab7+ endosomes ([C], [F], and [I]. Fraction of red fluorescence overlapping green is shown for each image (R ∈ G). Scale bars are 10 μm.

(J) Transfection with $Rab5^{Q79L}$-GFP does not block increase of the translocation ratio seen after treatment with dexamethasone, $5.3^{Dex}$, or $Arg_8^{Dex}$, but decreases the translocation ratio measured after treatment with $Tat^{Dex}$ ($p = 0.005$).

(K) HeLa cells were treated with 200 nM wortmannin for 30 min before treatment with 1 μM Dex, $5.3^{Dex}$, $Tat^{Dex}$, $Arg_8^{Dex}$, or $aPP^{Dex}$ for 30 additional min in the continued presence of the drug. Wortmannin decreased the translocation ratio measured after treatment with $Tat^{Dex}$ ($p = 8.1 \times 10^{-15}$) and $Arg_8^{Dex}$ ($p = 2.3 \times 10^{-5}$). Error bars shown represent mean ± SE. *ns*, not significant; *$p \leq 0.05$; **$p \leq 0.01$; ***$p \leq 0.001$, ANOVA with Bonferroni post-test.

See also Figure S5.

treated with $5.3^R$ showed that nearly all (95%) of the miniature protein localized to enlarged GFP+ endosomes (Figure 5B), suggesting that arresting early endosome maturation arrests trafficking of $5.3^R$ at the Rab5+ stage. Similar results were seen with $Arg_8^R$ and $Tat^R$ (Figures 5D–5I). These data suggest that $5.3^R$, $Tat^R$, and $Arg_8^R$ follow a shared path through Rab5+ and then Rab7+ vesicles and provide a starting point to ask which, if any, of these trafficking events are required to reach the cytoplasm.

To identify the point or points along the endocytic pathway at which these three molecules escape to the cytsosol, we blocked vesicle maturation through overexpression of $Rab5^{Q79L}$-GFP and assayed for cytosolic localization using dual-color microscopy and an orthogonally labeled GR-mCherry (Figure 5J). The TR of untreated HeLa cells expressing $Rab5^{Q79L}$-GFP or Rab5-GFP and GR-mCherry was near unity (TR = 1.32 ± 0.07), as expected, and remained unchanged after treatment for 30 min with 1 μM $aPP^{Dex}$ (TR = 1.25 ± 0.04). As expected, the TR values of $Rab5^{Q79L}$-GFP- and Rab5-GFP-expressing cells increased after treatment for 30 min with 1 μM of Dex (TR = 2.45 ± 0.21 and 2.24 ± 0.15 for Rab5-GFP- and $Rab5^{Q79L}$-GFP-expressing cells, respectively). Treatment with 1 μM $5.3^{Dex}$ resulted in TR values that were similar regardless of whether cells were transfected with wild-type Rab5-GFP or $Rab5^{Q79L}$-GFP (1.80 ± 0.08 versus 1.90 ± 0.07, respectively); similar findings were observed when cells were treated with $Arg_8^{Dex}$ (1.59 ± 0.11 versus 1.60 ± 0.09, respectively). By contrast, treatment with $Tat^{Dex}$ resulted in TR values that differed depending on whether cells were transfected with wild-type Rab5-GFP or $Rab5^{Q79L}$-GFP (1.57 ± 0.04 versus 1.26 ± 0.03, respectively; $p = 0.0057$). Thus, arresting vesicle maturation with the GTPase-inactive Rab5 mutant $Rab5^{Q79L}$ blocked the ability of $Tat^{Dex}$ to reach the cytoplasm but had no effect on $5.3^{Dex}$ or $Arg_8^{Dex}$. These findings suggest that 5.3 and $Arg_8$ escape to the cytoplasm from Rab5+ vesicles, whereas Tat can only escape later along the endocytic pathway.

To arrest endocytic traffic at an earlier stage, we treated cells with 200 nM wortmannin, a pharmacologic inhibitor of PI3K that blocks the maturation of Rab5+ vesicles (Christoforidis et al., 1999a) by decreasing the recruitment of Rab5 effectors that bind simultaneously to Rab5 and PI-3-phosphate-containing membranes (Zoncu et al., 2009). Wortmannin treatment blocked the increase in TR seen after treatment with $Tat^{Dex}$ and $Arg_8^{Dex}$ by 72% and 77%, respectively (Figure 5K). In contrast, the TR increase seen after treatment with $5.3^{Dex}$ in the presence or absence of wortmannin was similar (2.36 ± 0.08 versus 2.76 ± 0.10), confirming that $5.3^{Dex}$ escapes at or before the earliest Rab5+ state. Taken together, these data suggest that arresting vesicle maturation inhibits the cytosolic access of both $Tat^{Dex}$ and $Arg_8^{Dex}$, but that $5.3^{Dex}$ is capable of leaving these earliest vesicles and reaching the cytoplasm.

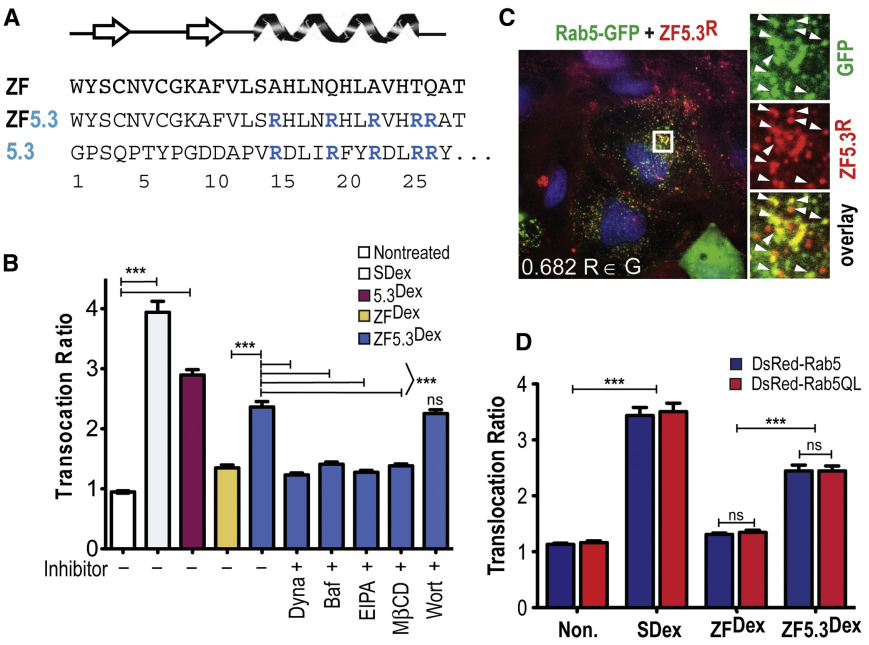


**Figure 6. The 5.3 Arginine Motif Is Transportable**

(A) Primary sequences of a zinc finger domain (ZF) and an analogous domain in which all five arginines have been substituted with alanine (ZF5.3).

(B) Translocation of GR-GFP after treatment with 1 μM SDex or the indicated Dex-labeled molecule in the presence and absence of endocytic inhibitors, as described in Figure 5.

(C) Colocalization of Rab5-GFP (green) with ZF5.3R (red) and Hoescht 33342 (blue).

(D) Rab5Q79L-GFP overexpression does not block increase of the translocation ratio seen after treatment with ZF5.3$^{Dex}$. Error bars shown represent mean ± standard error. *ns*, not significant; ***p < 0.001, ANOVA with Bonferroni post-test. See also Figure S6.

## Increased Cytosolic Localization of Zinc Finger Proteins Modified with 5.3 Arg Motif

The results described above suggest that the arginine motif present in the aPP variant 5.3 facilitates the release of this molecule from Rab5+ endosomes into the cytosol. Notably, the regioisomer 5.2, although also decorated with five arginine side chains on the external α-helix face, is released much less efficiently (Figure 3). To determine whether the arginine motif present on the 5.3 α-helix is transportable, that is, whether it can promote the cytosolic localization of other α-helix-containing proteins, we turned to the zinc finger proteins, as their therapeutic potential is well known (Sera, 2009; Urnov et al., 2010). We began with the sequence of CP1, a single zinc finger possessing high zinc ion affinity (Krizek et al., 1991), and prepared a dexamethasone-labeled variant (ZF5.3$^{Dex}$) whose α-helix was substituted with the arginine motif in 5.3 (Figure 6A), a change that neither prevented zinc binding nor significantly changed the secondary structure as measured by CD (Figure S6A). We next evaluated the extent to which ZF5.3$^{Dex}$ induced the nuclear translocation of GR-GFP when compared with a variant lacking the arginine motif (ZF$^{Dex}$) (Figure 6B). Treatment of HeLa cells expressing GR-GFP with 1 μM ZF5.3$^{Dex}$ for 30 min led to a large increase in TR (2.4 ± 0.09) compared to both an untreated sample (0.9 ± 0.05) and one treated with ZF$^{Dex}$ (1.4 ± 0.05) ($p < 0.0001$, ANOVA with Bonferroni post-test). Control experiments confirmed that ZF5.3$^{R}$ can be recovered from cytosolic extracts of HeLa cells treated with ZF5.3$^{R}$ (Figure S3L), and that the peptide backbone of ZF5.3 is not significantly degraded under the conditions in this assay (Figure S6I). As observed with 5.3, inhibition of early endocytic events with dynasore, bafilomycin, EIPA, or methyl-β-cyclodextrin reduced to background levels the increase in translocation ratios observed in the presence of ZF5.3$^{Dex}$ (Figure 6B). Furthermore, as observed with 5.3, when cells expressing GFP-Rab5 were treated with ZF5.3$^{R}$ and examined by confocal microscopy, 68% of the rhodamine channel overlapped with the signal from GFP-Rab5, confirming that ZF5.3$^{R}$ is present in Rab5+ vesicles (Figure 6C). Finally, as observed with 5.3, the TR of cells treated with ZF5.3$^{R}$ was unaffected when endocytic traffic was arrested by treatment with wortmannin or overexpression of dominant-negative Rab5$^{Q79L}$-GFP (Figures 6B and 6D). Together, these data imply that the arginine motif in ZF5.3, like the arginine motif in 5.3, functions to promote endocytic uptake and release from early Rab5+ endosomes, and emphasizes the potential of helical-arginine display for modulating the escape of cationic miniature proteins and peptidomimetics from early endosomes into the cytoplasm. Although further work is necessary to evaluate how broadly the motif identified here can be applied, these results provide a structural and mechanistic framework for efficiently increasing the cell permeabilities of therapeutic peptides and proteins. We estimate that between 1% and 5% of the intracellular pool of 5.3 and ZF5.3 enters the cytosol.

## DISCUSSION

The interfaces that form between and among proteins and DNA—often large, flat, and polar—do not often resemble those that bind small-molecule substrates or traditional inhibitors (Rutledge et al., 2003). Targeting these "undruggable" interfaces is a task well suited to protein and peptide ligands but can only be successful if such molecules reach their cytosolic targets. Unfortunately, the very properties that endow peptide mimetics with their promise—size and polarity—are precisely those properties forbidden by Lipinski's rules (Lipinski et al., 2001). The challenge, therefore, is to identify the determinants that guide the uptake of peptide-like molecules and the mechanisms through which they gain cytosolic access, generating a new set of rules applicable to large peptidic molecules and their mimetics. Advancing this goal has been constrained by the absence of a rapid and robust assay capable of distinguishing between peptide-like molecules that remain trapped within endosomes and those that escape into the cytosol.

Here we took advantage of developments in automated image analysis and the rapid cytoplasmic-to-nuclear translocation of

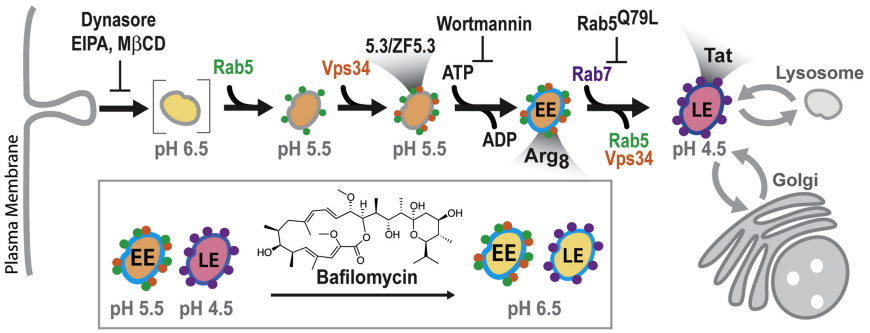


**Figure 7. Scheme Illustrating the Stepwise Pathway of Traffic Taken by 5.3, ZF5.3, Tat, and $Arg_8$ from the Cell Exterior into the Cytosol**

The path taken by 5.3, ZF5.3, Tat and Arg8 from the cell exterior to the cytosol begins with and requires endocytosis from the plasma membrane. 5.3, ZF5.3, Tat, and Arg8 bind to the cell surface and traffic into early endosomes, which rapidly acquire Rab5, followed by Vps34, a lipid kinase responsible for generating PI3P. Inhibition of Vps34 by Wortmannin fails to block escape of 5.3 or ZF5.3 (see Figures 5 and 6), indicating these molecules can escape vesicles prior to this stage. Rab5 and PI3P recruit Rab5 effectors, beginning endosome maturation. Recruitment of Rab7 leads to the formation of late endosomes (LE). The Rab5+-to-Rab7+ transition, which is blocked following transfection with Rab5Q79L, is not required for 5.3 or ZF5.3 to access the cytoplasm, but decreases the escape of Tat (see Figure 5), suggesting Tat escapes later in the endocytic pathway. Arg8 escape is blocked by wortmannin treatment but not by transfection with Rab5Q79L, suggesting escape begins late in the Rab5 stage but prior to the Rab7 stage. Endosomes are progressively acidified, a process blocked by bafilomycin (structure shown) and required for 5.3, ZF5.3, Tat, and $Arg_8$ to reach the cytoplasm.

the GR to develop an assay that, by monitoring nuclear accumulation of a GR-GFP fusion, reports on the cytoplasmic entry of traditionally impermeant molecules tagged with the GR ligand Dex. This assay offers advantages in both speed and cost over a first-generation assay developed by Kodadek and colleagues (Yu et al., 2005), as it provides a readout in individual living cells within 30 min (as opposed to 48 hr) and eliminates the requirement for cell lysis or costly enzymatic substrates. With this assay, we measured differences in the cytosolic localization of four actively endocytosed miniature proteins and identified 5.3 and ZF5.3 as minimally cationic proteins whose rapid cytosolic localization is equivalent to or better than Tat and $Arg_8$. Furthermore, 68 of 71 cells (96%) treated with 5.3Dex showed significant changes in GR-GFP localization, whereas only 2 of 55 cells treated with Dex-aPP (3.6%) showed increased translocation ratios, highlighting that minimally cationic protein domains containing the 5.3 motif enter the cytoplasm of most cells. The large differences in cytosolic localization among the set of closely related miniature proteins emphasize that distinct structural determinants control both endocytic uptake and endosomal release. Both 5.2 and 5.3 possess mass to charge ratios of 0.73 charge units per kDa, near the value suggested by Cronican et al. (2011) to predict cell penetrating activity, but less than +36 GFP (+1.27/kDa). Nevertheless, even among proteins with similar mass to charge ratios, uptake appears to be favored by clustered $\alpha$-helical arginine side chains, whereas release requires a more dispersed arginine array.

Coupling this new assay for cytosolic localization with live-cell confocal microscopy allowed us to further clarify contrasting models for the intracellular pathway taken by cationic miniature proteins and peptides en route to the cytoplasm. At low concentrations, none of the molecules studied here crossed the plasma membrane directly. Miniature protein 5.3 and the zinc finger module ZF5.3 enter into and escape from early (Rab5+) endosomes. In contrast, Tat and $Arg_8$, which are also present in Rab5+ vesicles, require delivery to downstream Rab7+ vesicles or the recruitment of Rab5 effectors in order to reach the cytoplasm (Figure 7). The differences in arginine/lysine number and orientation in 5.3, ZF5.3, Tat, and $Arg_8$ will likely affect their side chain p*K*a values and thus the overall charge of each molecule at any given pH. Thus, it is possible that the distinct arginine array in 5.3 and ZF5.3 favors formation of a critical protonated species within the early endosome (pH ~6.5), whereas the lower pH present in lysosomes may be required to generate an equivalent state for Tat and $Arg_8$. Alternatively, the distinct arginine array in 5.3 and ZF5.3 could represent an export signal for cellular machinery that has yet to be identified.

## SIGNIFICANCE

**Proteins and other peptidic molecules able to cross biological membranes possess promise both as therapeutics and as agents for delivery of macromolecules, such as siRNA, to the cytoplasm of target cells. In a broader sense, proteins and peptides that effectively traffic across membranes offer the potential to illuminate fundamental principles of cell biology. In this work we identified two small folded proteins, the cationic miniature protein 5.3 and the zinc finger module ZF5.3, that achieve cytosolic access through rapid internalization and efficient escape from Rab5+ endosomes. The trafficking pathway that we mapped for these molecules is similar to that taken by botulinum and anthrax toxins, which also escape from early endosomes (Simpson, 2004). The pathways followed by Tat and $Arg_8$, however, resemble those of SV40 (Vonderheit and Helenius, 2005) and HIV-1 (Vidricaire and Tremblay, 2005) and require transport beyond early Rab5+ endosomes to gain cytosolic access. This difference in trafficking indicates that the ability of 5.3 and ZF5.3 to rapidly escape from early endosomes is a unique feature not shared by canonical cell-penetrating peptides, and it implies the existence of distinct signals, encodable within short peptide sequences, that favor early versus late endosomal release. Identifying these signals and understanding their mechanistic basis will illustrate how cells control the movement of endocytic cargo and may allow researchers to engineer molecules to follow a desired delivery pathway for rapid cytosolic access. Collectively, our investigations represent a starting point for the optimization of well-folded functional cell-penetrating proteins**

**useful as pharmacologic tools and capable of modulating cytoplasmic protein function.**

## EXPERIMENTAL PROCEDURES

### Cell Culture and Transfections

HeLa cells (ATCC, Manassas, VA) were grown in T-75 culture flasks containing Dulbecco's modified essential medium (DMEM; GIBCO Cat. #11995-065, Invitrogen, Carlsbad, CA) supplemented with 10% fetal bovine serum, and 100 U/ml each penicillin and streptomycin. Transient transfections were performed using Fugene 6 or XtremeGene HP (Roche, Indianapolis, IN) and protocols recommended by the manufacturer. Plasmids encoding Rab5-GFP and Rab5$^{Q79L}$-GFP were gifts from Pietro DeCamilli. A plasmid containing Rab7-GFP was a gift of Qing Zhong (plasmid #28047, Addgene, Cambridge, MA). A plasmid containing GalT-EGFP was a gift of Jeniffer Lippincott-Schwartz (Addgene plasmid #11937). A plasmid containing the glucocortcoid receptor fused to EGFP (pK7-GR-GFP) was a gift of Ian Macara (Addgene plasmid #15534).

### Analysis of Surface Binding and Cell Uptake

HeLa cells grown to ~90% confluency were dissociated from flasks by incubation for 15 min at 37°C with 2 ml PBS, 1 mM EDTA, and 1 mM EGTA. Cells were collected in warmed media, and aliquots (150 μl, 200,000 cells) distributed to 96 well plates. The cells were incubated at 4°C or 37°C for 10 min, 1 μM fluorescently labeled peptide was added, and incubation continued for an additional 30 min. Cells were then washed twice with DMEM + 10% fetal bovine serum and treated with trypsin (30 μl per well, 0.05%, 37°C × 10 min) before resuspending in 300 μl PBS. Cells were analyzed by flow cytometry using an Accuri C6 flow cytometer. To confirm that trypsin treatment removed fluorescently labeled peptide remaining on the cell surface, HeLa cells were treated with 1 μM miniature protein or peptide at 4°C to inhibit endocytosis. After washing twice, the cells were then treated with trypsin (30 μl, 0.05%, 37°C × 10 min) or PBS as a control. Cells were then resuspended in 300 μl PBS before analysis by flow cytometry. Data presented are the mean ± SEM for four biological replicates measuring the mean fluorescence intensity of 30,000 cells. Dead cells defined by forward and side scatter were excluded.

### Colocalization of Miniature Proteins with Alexa-488-Transferrin and Rab-GFP Fusions

To examine the colocalization of rhodamine-labeled miniature proteins or peptides with Alexa-488-transferrin (Tf$^{488}$), HeLa cells were plated (200 μl, $10^4$ cells/well, 96 well glass bottom plates, Matrical, Spokane, WA) the day prior to experiments. The media was replaced with 150 μl HEPES-Krebs-Ringer's (HKR) buffer (140 mM NaCl, 2 mM KCl, 1 mM $CaCl_2$, 1 mM $MgCl_2$, 10 mM HEPES [pH 7.4]) containing 1 μM hodamine-labeled molecule or 25 nM Alexa-488-transferrin (Molecular Probes, Eugene, OR) and the cells were incubated at 37°C for 30 min. The cells were then rinsed twice with 200 μl HKR buffer and nuclei were labeled by overlaying 200 μl HKR containing 300 nM Hoechst 33342 (Molecular Probes Cat. #H3570) for 5 min. Images of cells were acquired using a PerkinElmer (Waltham, MA) LiveView spinning disk confocal microscope fitted with a 60 × 1.2 NA objective. Colocalization with Rab-GFP fusions was examined in an analogous way using HeLa cells transfected with the appropriate expression plasmid. See Supplemental Experimental Procedures online for details.

### Effects of Inhibitors on Cell Uptake

HeLa cells grown for 24 hr in glass-bottom plates were incubated with HKR buffer or HKR buffer containing 80 μM dynasore, 50 μM N-ethyl-isopropyl-amiloride, or 5 mM methyl-β-cyclodextrin for 30 min at 37°C prior to the addition of 1 μM rhodamine-labeled miniature protein or peptide (Tat and $Arg_8$). The cells were washed twice with DMEM, the nuclei labeled with Hoescht, and images acquired as described above for colocalization experiments.

### GR-GFP Translocation Assay

HeLa cells transfected with pK7-GR-GFP were plated in Matrical plates as described above. To label nuclei, the media were replaced with HKR buffer containing 300 nM Hoescht 33342 and the cells were incubated for 30 min at 37°C. Cells were then treated with 150 μl HKR buffer or HKR buffer containing 1 μM dexamethasone, dexamethasone-labeled miniature protein, or dexamethasone-labeled peptides for 30 min at 37°C before epifluorescence imaging. The translocation ratio (the ratio of the median intensities of GFP in the nuclear and surrounding region) for each cell imaged was measured using CellProfiler (Carpenter et al., 2006). For further details see Supplemental Experimental Procedures online.

To examine the effects of various inhibitors, HeLa cells transfected and plated as above were pretreated with HKR buffer containing 300 nM Hoescht and 80 μM dynasore, 50 μM N-ethyl-isopropyl-amiloride, 200 nM wortmannin, 200 nM bafilomycin, or 5 mM methyl-β-cyclodextrin for 30 min at 37°C, after which 1 μM dexamethasone, dexamethasone-labeled miniature protein, or dexamethasone-labeled peptide was added for an additional 30 min at 37°C. Cells were then analyzed as described above.

To evaluate the requirement of Rab5 activity for the ability of peptides to reach the cytoplasm, HeLa cells were transfected with pGR-mCherry and either Rab5-EGFP or Rab5$^{Q79L}$-EGFP for 24 hr before treatment with dexamethasone or dexamethasone-labeled miniature proteins or peptides and imaging as described above. Cotransfected cells expressing Rab-GFP fusions and pGR-mCherry were identified via their characteristic pattern of green and red fluorescence. The translocation ratio was determined using median values of mCherry fluorescence within the nucleus and surrounding region using CellProfiler.

### Statistical Analysis

Comparisons within groups were made using ANOVA. Pairwise comparisons within groups were made using Bonferroni's post-test after finding a significant difference using ANOVA. P values are corrected using Bonferroni's method (Shaffer, 1995) so that the family-wise error rate is 0.05. Otherwise, comparisons were made using a two-tailed t test.

### Supplemental Experimental Procedures

Supplemental Experimental Procedures containing additional descriptions of materials, polypeptide synthesis and characterization, pGR-mCherry vector construction, circular dichroism analysis, and image acquisition and analysis may be found online.

## SUPPLEMENTAL INFORMATION

Supplemental Information contains six figures, one table, and Supplemental Experimental Procedures and can be found with this article online at http://dx.doi.org/10.1016/j.chembiol.2012.05.022.

## ACKNOWLEDGMENTS

We are grateful to the NIH for support of this work (GM 74756). Support for J.S.A. and D.M.B. was provided in part by NIH MSTP TG T32GM07205. J.S.A. was also supported by NIH F30 HL 09407803. Support for J.R.L. was provided by T32GM067543. A.S. is a member of the Scientific Advisory Board of Permeon Biologics.

Received: January 2, 2012
Revised: May 23, 2012
Accepted: May 25, 2012
Published: July 26, 2012

## REFERENCES

Androlewicz, M.J., Anderson, K.S., and Cresswell, P. (1993). Evidence that transporters associated with antigen processing translocate a major histocompatibility complex class I-binding peptide into the endoplasmic reticulum in an ATP-dependent manner. Proc. Natl. Acad. Sci. USA *90*, 9130–9134.

Belitsky, J.M., Leslie, S.J., Arora, P.S., Beerman, T.A., and Dervan, P.B. (2002). Cellular uptake of N-methylpyrrole/N-methylimidazole polyamide-dye conjugates. Bioorg. Med. Chem. *10*, 3313–3318.

 

Blundell, T.L., Pitts, J.E., Tickle, I.J., Wood, S.P., and Wu, C.W. (1981). X-ray analysis (1. 4-Å resolution) of avian pancreatic polypeptide: small globular protein hormone. Proc. Natl. Acad. Sci. USA *78*, 4175–4179.

Cantalupo, G., Alifano, P., Roberti, V., Bruni, C.B., and Bucci, C. (2001). Rab-interacting lysosomal protein (RILP): the Rab7 effector required for transport to lysosomes. EMBO J. *20*, 683–693.

Carey, K.L., Richards, S.A., Lounsbury, K.M., and Macara, I.G. (1996). Evidence using a green fluorescent protein-glucocorticoid receptor chimera that the Ran/TC4 GTPase mediates an essential function independent of nuclear protein import. J. Cell Biol. *133*, 985–996.

Carpenter, A.E., Jones, T.R., Lamprecht, M.R., Clarke, C., Kang, I.H., Friman, O., Guertin, D.A., Chang, J.H., Lindquist, R.A., Moffat, J., et al. (2006). CellProfiler: image analysis software for identifying and quantifying cell phenotypes. Genome Biol. *7*, R100.

Chin, J.W., and Schepartz, A. (2001). Design and evolution of a miniature Bcl-2 binding protein. Angew. Chem. Int. Ed. Engl. *40*, 3806–3809.

Christoforidis, S., McBride, H.M., Burgoyne, R.D., and Zerial, M. (1999a). The Rab5 effector EEA1 is a core component of endosome docking. Nature *397*, 621–625.

Christoforidis, S., Miaczynska, M., Ashman, K., Wilm, M., Zhao, L., Yip, S.C., Waterfield, M.D., Backer, J.M., and Zerial, M. (1999b). Phosphatidylinositol-3-OH kinases are Rab5 effectors. Nat. Cell Biol. *1*, 249–252.

Cole, N.B., Smith, C.L., Sciaky, N., Terasaki, M., Edidin, M., and Lippincott-Schwartz, J. (1996). Diffusional mobility of Golgi proteins in membranes of living cells. Science *273*, 797–801.

Cronican, J.J., Beier, K.T., Davis, T.N., Tseng, J.C., Li, W., Thompson, D.B., Shih, A.F., May, E.M., Cepko, C.L., Kung, A.L., et al. (2011). A class of human proteins that deliver functional proteins into mammalian cells in vitro and in vivo. Chem. Biol. *18*, 833–838.

Daniels, D.S., and Schepartz, A. (2007). Intrinsically cell-permeable miniature proteins based on a minimal cationic PPII motif. J. Am. Chem. Soc. *129*, 14578–14579.

Derossi, D., Calvet, S., Trembleau, A., Brunissen, A., Chassaing, G., and Prochiantz, A. (1996). Cell internalization of the third helix of the Antennapedia homeodomain is receptor-independent. J. Biol. Chem. *271*, 18188–18193.

Doherty, G.J., and McMahon, H.T. (2009). Mechanisms of endocytosis. Annu. Rev. Biochem. *78*, 857–902.

Duchardt, F., Fotin-Mleczek, M., Schwarz, H., Fischer, R., and Brock, R. (2007). A comprehensive model for the cellular uptake of cationic cell-penetrating peptides. Traffic *8*, 848–866.

Fernández-Suárez, M., and Ting, A.Y. (2008). Fluorescent probes for super-resolution imaging in living cells. Nat. Rev. Mol. Cell Biol. *9*, 929–943.

Fischer, P.M. (2007). Cellular uptake mechanisms and potential therapeutic utility of peptidic cell delivery vectors: progress 2001–2006. Med. Res. Rev. *27*, 755–795.

Fischer, R., Köhler, K., Fotin-Mleczek, M., and Brock, R. (2004). A stepwise dissection of the intracellular fate of cationic cell-penetrating peptides. J. Biol. Chem. *279*, 12625–12635.

Frankel, A.D., and Pabo, C.O. (1988). Cellular uptake of the tat protein from human immunodeficiency virus. Cell *55*, 1189–1193.

Futaki, S., Suzuki, T., Ohashi, W., Yagami, T., Tanaka, S., Ueda, K., and Sugiura, Y. (2001). Arginine-rich peptides. An abundant source of membrane-permeable peptides having potential as carriers for intracellular protein delivery. J. Biol. Chem. *276*, 5836–5840.

Gemperli, A.C., Rutledge, S.E., Maranda, A., and Schepartz, A. (2005). Paralog-selective ligands for bcl-2 proteins. J. Am. Chem. Soc. *127*, 1596–1597.

Golemi-Kotra, D., Mahaffy, R., Footer, M.J., Holtzman, J.H., Pollard, T.D., Theriot, J.A., and Schepartz, A. (2004). High affinity, paralog-specific recognition of the Mena EVH1 domain by a miniature protein. J. Am. Chem. Soc. *126*, 4–5.

Hanover, J.A., Willingham, M.C., and Pastan, I. (1984). Kinetics of transit of transferrin and epidermal growth factor through clathrin-coated membranes. Cell *39*, 283–293.

Hodges, A.M., and Schepartz, A. (2007). Engineering a monomeric miniature protein. J. Am. Chem. Soc. *129*, 11024–11025.

Huotari, J., and Helenius, A. (2011). Endosome maturation. EMBO J. *30*, 3481–3500.

Johannes, L., and Popoff, V. (2008). Tracing the retrograde route in protein trafficking. Cell *135*, 1175–1187.

Johnson, R.M., Harrison, S.D., and Maclean, D. (2011). Therapeutic applications of cell-penetrating peptides. Methods Mol. Biol. *683*, 535–551.

Krizek, B.A., Amann, B.T., Kilfoil, V.J., Merkle, D.L., and Berg, J.M. (1991). A consensus zinc finger peptide: design, high-affinity metal binding, a pH-dependent structure, and a His to Cys sequence variant. J. Am. Chem. Soc. *113*, 4518–4523.

Koivusalo, M., Welch, C., Hayashi, H., Scott, C.C., Kim, M., Alexander, T., Touret, N., Hahn, K.M., and Grinstein, S. (2010). Amiloride inhibits macropinocytosis by lowering submembranous pH and preventing Rac1 and Cdc42 signaling. J. Cell Biol. *188*, 547–563.

Lakadamyali, M., Rust, M.J., and Zhuang, X. (2006). Ligands for clathrin-mediated endocytosis are differentially sorted into distinct populations of early endosomes. Cell *124*, 997–1009.

Lipinski, C.A., Lombardo, F., Dominy, B.W., and Feeney, P.J. (2001). Experimental and computational approaches to estimate solubility and permeability in drug discovery and development settings. Adv. Drug Deliv. Rev. *46*, 3–26.

Luedtke, N.W., Carmichael, P., and Tor, Y. (2003). Cellular uptake of aminoglycosides, guanidinoglycosides, and poly-arginine. J. Am. Chem. Soc. *125*, 12374–12375.

Macia, E., Ehrlich, M., Massol, R., Boucrot, E., Brunner, C., and Kirchhausen, T. (2006). Dynasore, a cell-permeable inhibitor of dynamin. Dev. Cell *10*, 839–850.

Maiolo, J.R., 3rd, Ottinger, E.A., and Ferrer, M. (2004). Specific redistribution of cell-penetrating peptides from endosomes to the cytoplasm and nucleus upon laser illumination. J. Am. Chem. Soc. *126*, 15376–15377.

Moya-Ortega, M.D., Alvarez-Lorenzo, C., Sigurdsson, H.H., Concheiro, A., and Loftsson, T. (2010). Gamma-cyclodextrin hydrogels and semi-interpenetrating networks for sustained delivery of dexamethasone. Carbohydr. Polym. *80*, 900–907.

Palm, C., Jayamanne, M., Kjellander, M., and Hällbrink, M. (2007). Peptide degradation is a critical determinant for cell-penetrating peptide uptake. Biochim. Biophys. Acta *1768*, 1769–1776.

Palm-Apergi, C., Lorents, A., Padari, K., Pooga, M., and Hällbrink, M. (2009). The membrane repair response masks membrane disturbances caused by cell-penetrating peptide uptake. FASEB J. *23*, 214–223.

Payne, C.K., Jones, S.A., Chen, C., and Zhuang, X. (2007). Internalization and trafficking of cell surface proteoglycans and proteoglycan-binding ligands. Traffic *8*, 389–401.

Puthenveedu, M.A., Lauffer, B., Temkin, P., Vistein, R., Carlton, P., Thorn, K., Taunton, J., Weiner, O.D., Parton, R.G., and von Zastrow, M. (2010). Sequence-dependent sorting of recycling proteins by actin-stabilized endosomal microdomains. Cell *143*, 761–773.

Richard, J.P., Melikov, K., Vives, E., Ramos, C., Verbeure, B., Gait, M.J., Chernomordik, L.V., and Lebleu, B. (2003). Cell-penetrating peptides. A reevaluation of the mechanism of cellular uptake. J. Biol. Chem. *278*, 585–590.

Rink, J., Ghigo, E., Kalaidzidis, Y., and Zerial, M. (2005). Rab conversion as a mechanism of progression from early to late endosomes. Cell *122*, 735–749.

Rodal, S.K., Skretting, G., Garred, O., Vilhardt, F., van Deurs, B., and Sandvig, K. (1999). Extraction of cholesterol with methyl-beta-cyclodextrin perturbs formation of clathrin-coated endocytic vesicles. Mol. Biol. Cell *10*, 961–974.

Rothbard, J.B., Jessop, T.C., and Wender, P.A. (2005). Adaptive translocation: the role of hydrogen bonding and membrane potential in the uptake of guanidinium-rich transporters into cells. Adv. Drug Deliv. Rev. *57*, 495–504.

Rutledge, S.E., Volkman, H.M., and Schepartz, A. (2003). Molecular recognition of protein surfaces: high affinity ligands for the CBP KIX domain. J. Am. Chem. Soc. *125*, 14336–14347.

Ryser, H.J., and Hancock, R. (1965). Histones and basic polyamino acids stimulate the uptake of albumin by tumor cells in culture. Science *150*, 501–503.

Sera, T. (2009). Zinc-finger-based artificial transcription factors and their applications. Adv. Drug Deliv. Rev. *61*, 513–526.

Shaffer, J. (1995). Multiple hypothesis testing. Annu. Rev. Psychol. *46*, 561–584.

Simpson, L.L. (2004). Identification of the major steps in botulinum toxin action. Annu. Rev. Pharmacol. Toxicol. *44*, 167–193.

Smith, B.A., Daniels, D.S., Coplin, A.E., Jordan, G.E., McGregor, L.M., and Schepartz, A. (2008). Minimally cationic cell-permeable miniature proteins via α-helical arginine display. J. Am. Chem. Soc. *130*, 2948–2949.

Stenmark, H., Parton, R.G., Steele-Mortimer, O., Lütcke, A., Gruenberg, J., and Zerial, M. (1994). Inhibition of rab5 GTPase activity stimulates membrane fusion in endocytosis. EMBO J. *13*, 1287–1296.

Strohl, W.R., and Knight, D.M. (2009). Discovery and development of biopharmaceuticals: current issues. Curr. Opin. Biotechnol. *20*, 668–672.

Ter-Avetisyan, G., Tünnemann, G., Nowak, D., Nitschke, M., Herrmann, A., Drab, M., and Cardoso, M.C. (2009). Cell entry of arginine-rich peptides is independent of endocytosis. J. Biol. Chem. *284*, 3370–3378. Published online December 1, 2008. 10.1074/jbc.M805550200.

Théodore, L., Derossi, D., Chassaing, G., Llirbat, B., Kubes, M., Jordan, P., Chneiweiss, H., Godement, P., and Prochiantz, A. (1995). Intraneuronal delivery of protein kinase C pseudosubstrate leads to growth cone collapse. J. Neurosci. *15*, 7158–7167.

Urnov, F.D., Rebar, E.J., Holmes, M.C., Zhang, H.S., and Gregory, P.D. (2010). Genome editing with engineered zinc finger nucleases. Nat. Rev. Genet. *11*, 636–646.

Verdine, G.L., and Hilinski, G.J. (2012). All-hydrocarbon stapled peptides as synthetic cell-accessible mini-proteins. Drug Discov. Today Technol. *9*, e41–e47.

Vidricaire, G., and Tremblay, M.J. (2005). Rab5 and Rab7, but not ARF6, govern the early events of HIV-1 infection in polarized human placental cells. J. Immunol. *175*, 6517–6530.

Vonderheit, A., and Helenius, A. (2005). Rab7 associates with early endosomes to mediate sorting and transport of Semliki forest virus to late endosomes. PLoS Biol. *3*, e233.

Wadia, J.S., Stan, R.V., and Dowdy, S.F. (2004). Transducible TAT-HA fusogenic peptide enhances escape of TAT-fusion proteins after lipid raft macropinocytosis. Nat. Med. *10*, 310–315.

Wender, P.A., Galliher, W.C., Goun, E.A., Jones, L.R., and Pillow, T.H. (2008). The design of guanidinium-rich transporters and their internalization mechanisms. Adv. Drug Deliv. Rev. *60*, 452–472.

White, T.R., Renzelman, C.M., Rand, A.C., Rezai, T., McEwan, C.M., Gelev, V.M., Turner, R.A., Linington, R.G., Leung, S.S.F., Kalgutkar, A.S., et al. (2011). On-resin N-methylation of cyclic peptides for discovery of orally available scaffolds. Nat. Chem. Bio. *7*, 810–817.

Yoshimori, T., Yamamoto, A., Moriyama, Y., Futai, M., and Tashiro, Y. (1991). Bafilomycin A1, a specific inhibitor of vacuolar-type $H^+$-ATPase, inhibits acidification and protein degradation in lysosomes of cultured cells. J. Biol. Chem. *266*, 17707–17712.

Yu, H., Zou, Y., Wang, Y., Huang, X., Huang, G., Sumer, B.D., Boothman, D.A., and Gao, J. (2011). Overcoming endosomal barrier by amphotericin B-loaded dual pH-responsive PDMA-b-PDPA micelleplexes for siRNA delivery. ACS Nano *5*, 9246–9255.

Yu, P., Liu, B., and Kodadek, T. (2005). A high-throughput assay for assessing the cell permeability of combinatorial libraries. Nat. Biotechnol. *23*, 746–751.

Zeigerer, A., Gilleron, J., Bogorad, R.L., Marsico, G., Nonaka, H., Seifert, S., Epstein-Barash, H., Kuchimanchi, S., Peng, C.G., Ruda, V.M., et al. (2012). Rab5 is necessary for the biogenesis of the endolysosomal system in vivo. Nature *485*, 465–470.

Zellefrow, C.D., Griffiths, J.S., Saha, S., Hodges, A.M., Goodman, J.L., Paulk, J., Kritzer, J.A., and Schepartz, A. (2006). Encodable activators of SRC family kinases. J. Am. Chem. Soc. *128*, 16506–16507.

Zhou, H., Wu, S., Joo, J.Y., Zhu, S., Han, D.W., Lin, T., Trauger, S., Bien, G., Yao, S., Zhu, Y., et al. (2009). Generation of induced pluripotent stem cells using recombinant proteins. Cell Stem Cell *4*, 381–384.

Zoncu, R., Perera, R.M., Balkin, D.M., Pirruccello, M., Toomre, D., and De Camilli, P. (2009). A phosphoinositide switch controls the maturation and signaling properties of APPL endosomes. Cell *136*, 1110–1121.

Zondlo, N.J., and Schepartz, A. (1999). Highly specific DNA recognition by a designed miniature protein. J. Am. Chem. Soc. *121*, 6938–6939.

## Note Added in Proof

It was recently reported by Barbas and coworkers that certain combinations of zinc finger modules can traffic to the nuclei of mammalian cells (Gaj, T. Guo, J., Kato, Y., Sirk, S.J., Barbas, C.F. III. Nature Meth. 10.1038/nmeth.2030).